FROM CELLULAR AUTOMATON RULES TO A MACROSCOPIC MEAN-FIELD DESCRIPTION*

H. Hatzikirou, L. Brusch, A. Deutsch

Center for Information Services and High Performance Computing
Technische Universität Dresden
Nöthnitzerstr. 46, 01069 Dresden, Germany
haralambos.hatzikirou@tu-dresden.de

Cellular automata (CA) may be viewed as simple models of self-organizing complex systems. Here, we focus on an important class of CA, the so-called lattice-gas cellular automata (LGCA), which have been proposed as models of spatio-temporal pattern formation in biology. As an example, we introduce a LGCA model for a simple biological growth process based on randomly moving and proliferating agents. We demonstrate how a mean-field approximation can yield insight into the formation of spatial patterns and calculate important macroscopic observables for the biological growth process. In particular, we address the role of the diffusion strength in the approximation by distinguishing well-stirred and spatially distributed cases. Finally, we discuss the potential and limitations of the mean-field description in analyzing biological pattern formation.

PACS numbers: 87.17.Aa, 87.10.Hk, 05.50.+q

1. Introduction

Cellular automata (CA) are discrete dynamical systems. They were introduced by J. von Neumann and S. Ulam in the 1950s in an attempt to model biological self-reproduction [16]. Since then, it has become clear that CA have a much broader potential as models for physical, chemical and biological systems. In particular, CA models have been proposed for a large number of biological applications for studying the emergence of collective macroscopic behavior arising from the microscopic interaction of individual components, such as molecules, cells or organisms [5]. However, currently there exists a huge jungle of different rules for often the same or

---

* Presented at the Summer Solstice 2009 International Conference on Discrete Models of Complex Systems, Gdańsk, Poland, June 22–24, 2009.

similar processes (*e.g.* random walk or proliferation). Therefore, there is need for a specification and classification of CA rules. Such a classification approach has comprehensively been performed for one-dimensional automata [18]. Furthermore, examples of successful analysis of CA models beyond purely visual inspection of simulation outcomes are still rare.

Here, we introduce lattice-gas cellular automata as models for collective behavior emerging from microscopic migration and interaction processes [5, 8]. LGCA represent a class of CA whose structure facilitates mathematical analysis. Implementing movement of individuals in traditional cellular automaton models is not straightforward, as one site in a lattice can typically only contain one individual, and consequently movement of individuals cause collisions when two individuals move to the same empty site. Classical CAs tackle the same problem in different ways, where a several of them are described in [1]. In a lattice-gas model this problem is avoided by having separate channels for each direction of movement and imposing an exclusion principle (Fig. 1). Furthermore, the update rule is split into two parts which are called interaction and propagation, respectively.
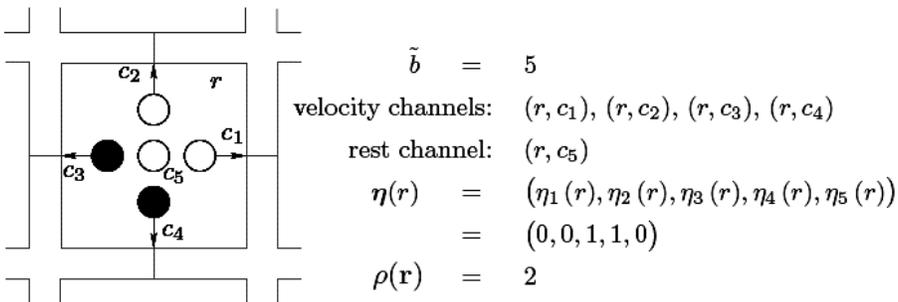

$$\tilde{b} = 5$$
velocity channels: $(r, c_1), (r, c_2), (r, c_3), (r, c_4)$
rest channel: (r, c_5)
$$\eta(r) = (\eta_1(r), \eta_2(r), \eta_3(r), \eta_4(r), \eta_5(r))$$
$$= (0, 0, 1, 1, 0)$$
$$\rho(\mathbf{r}) = 2$$

Fig. 1. Example of node configuration in a lattice-gas cellular automata: channels of node r in a two-dimensional square lattice ($b = 4$) with one rest channel ($\beta = 1$). Gray dots denote the presence of a particle in the respective channel.

The interaction rule of LGCA can be compared with the update rule for CA in that it assigns new states to each particle based on the states of the sites in a local neighborhood. After the interaction step the state of each node is propagated to a neighboring node (Fig. 2). This split of the update rule allows for transport of particles while keeping the rules simple. The emergent collective behavior, *e.g.* spatio-temporal pattern formation in a LGCA shows up in the macroscopic limit which can be derived from a theory of statistical mechanics on a lattice, *e.g.* [12, 17]. In place of discrete particles, Lattice Boltzmann (LB) models deal with continuous distribution functions which interact locally and which propagate after collision to the next neighbor node. LB models can be interpreted as mean-field approximations of
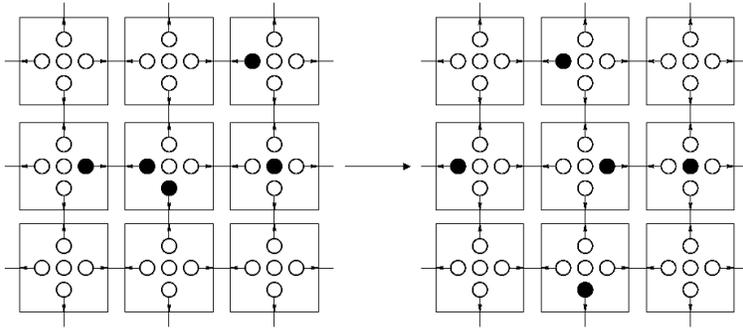
Fig. 2. Propagation in a two-dimensional square lattice-gas cellular automata with speed $m = 1$; lattice configurations before and after the propagation step; black dots denote the presence of a particle in the respective channel.

LGCA. LGCA and LB models have been originally introduced as models of fluid flow [8]. Meanwhile, LGCA and LB models have found numerous applications in physics, chemistry and more recently biology [3–6, 14].

In particular, LGCA have been proposed as mathematical models for biological pattern formation. For a selection of biology-motivated interactions, it has been shown in a recent book [5] that a corresponding lattice-Boltzmann approximation can be adopted to analyze the emergence of spatio-temporal patterns. The central step is the derivation of a spatio-temporal mean-field approximation of the automaton stochastic process. However, completely disregarding the spatial aspect would lead to qualitatively false model predictions as highlighted in a book review by Boerlijst [2]. Therein, a LGCA model for a simple growth process is approximated by a purely temporal description, the logistic equation, which is then analyzed to demonstrate the qualitative failure of the purely temporal approximation.

In this paper, inspired by the interesting discussion in [2], we provide an example of spatio-temporal insight to be gained from a mean-field finite-difference lattice-Boltzmann equation which we derive for a logistic growth process. We will directly compare two approximations with the results of stochastic LGCA simulations. First, under the assumption of a well-stirred system, we derive the temporal mean-field equation of the LGCA. Then, assuming finite diffusion strength and based on the spatio-temporal mean-field description of the microscopic growth process, we calculate by means of a Chapman–Enskog expansion technique the corresponding macroscopic partial differential equation (PDE), which is a reaction-diffusion equation of Fisher–Kolmogorov type [7]. Simulation results of the LGCA are found to be in very good agreement with the mean-field PDE, in contrast to the purely temporal mean-field approximation. From this mean-field PDE we

calculate important macroscopic observables of biological growth, such as total number of particles and *per capita* growth rate, and we reveal their dependence on the microscopic growth and transport parameters. Finally, we discuss the potential and limits of the proposed methodology.

2. The model

In this section, we define a LGCA model for a biological growth process. In particular, we will present the model assumptions and simplifications.

2.1. Notations and nomenclature

We consider a lattice-gas cellular automaton [5] defined on a two-dimensional regular lattice $\mathcal{L} = \{1 \ldots L_1\} \times \{1 \ldots L_2\} \subset \mathbb{Z}^2$, where L_1, L_2 are the lattice dimensions. Particles[1] move on the discrete lattice with discrete velocities, *i.e.* they hop at discrete time steps from a given node to a neighboring one, as determined by the *single particle speed*. The set of velocities for the square lattice as considered here, is represented by the two-dimensional channel velocity vectors:

$$\boldsymbol{c}_1 = \begin{pmatrix} 1 \\ 0 \end{pmatrix}, \ \boldsymbol{c}_2 = \begin{pmatrix} 0 \\ 1 \end{pmatrix}, \ \boldsymbol{c}_3 = \begin{pmatrix} -1 \\ 0 \end{pmatrix}, \ \boldsymbol{c}_4 = \begin{pmatrix} 0 \\ -1 \end{pmatrix}, \ \boldsymbol{c}_5 = \begin{pmatrix} 0 \\ 0 \end{pmatrix}.$$

In each of these channels, we consider an exclusion principle, *i.e.* we allow at most one particle per channel. We denote by $\tilde{b} = b + \beta$ the total number of channels per node which can be occupied simultaneously, where β is the number of channels with zero velocity, the so-called rest channels (see Fig. 1). The parameter b is the *coordination number*, *i.e.* the number of velocity channels on a node. We represent the channel occupancy by a Boolean random variable called *occupation number* $\eta_i(\boldsymbol{r}, k) \in \{0, 1\}$, where $i = 1, \ldots, \tilde{b}$, $\boldsymbol{r} = (r_x, r_y) \in \mathcal{L} \subset \mathbb{Z}^2$ the spatial variable and $k \in \mathbb{N}$ the time variable. The $\tilde{b}$-dimensional vector

$$\boldsymbol{\eta}(\boldsymbol{r}, k) := (\eta_1(\boldsymbol{r}, k), \ldots, \eta_{\tilde{b}}(\boldsymbol{r}, k)) \in \mathcal{E}$$

is called *node configuration* and $\mathcal{E} = \{0, 1\}^{\tilde{b}}$ the automaton *state space*. *Node density* is the total number of particles present at a node $\boldsymbol{r} \in \mathcal{L}$, and denoted by:

$$n(\boldsymbol{r}, k) := \sum_{i=1}^{\tilde{b}} \eta_i(\boldsymbol{r}, k).$$

---

[1] LGCA models are individual-based models. Although our model has a biological motivation through the proliferation of cells, we are going to use the term particle instead of cells. The reason is that our model definition is not "cell specific" and can be equally well used for physical particles or other proliferating individuals.

2.2. LGCA dynamics

In our automaton model, particle dynamics are defined by rules. Automaton dynamics arise from the application of three rules (operators): Propagation (P), reorientation (O) and growth (R). In particular, the reorientation and the propagation operators describe particle motion while the growth operator controls the change of the local number of particles on a node. In the following, we present these operators in detail.

2.2.1. Propagation (P)

The process of particle movement is modeled by the propagation step. The propagation step is deterministic and it is governed by an operator P. By the application of P all particles are transported simultaneously to nodes in the direction of their velocity, *i.e.* a particle residing in channel $(\boldsymbol{r}, \boldsymbol{c}_i)$ at time k is moved to a neighboring channel $(\boldsymbol{r} + m\boldsymbol{c}_i, \boldsymbol{c}_i)$ during one time step (Fig. 2). Here $m \in \mathbb{N}$ determines the speed and $m\boldsymbol{c}_i$ is the translocation of the particle. The particles residing on the rest channel do not move since they have zero velocity. In terms of occupation numbers, the state of a channel $(\boldsymbol{r} + m\boldsymbol{c}_i, \boldsymbol{c}_i)$ after propagation becomes:

$$\eta_i(\boldsymbol{r} + m\boldsymbol{c}_i, k + \tau) = \eta_i^{\mathrm{P}}(\boldsymbol{r} + m\boldsymbol{c}_i, k) = \eta_i(\boldsymbol{r}, k)\,,$$

where $\tau \in \mathbb{N}$ is the automaton's time-step. We note that this operator is mass and momentum conserving.

2.2.2. Reorientation (O)

The reorientation operator is responsible for the redistribution of particles within the velocity channels of a node, providing a new node velocity distribution. Here, we assume that the particles are just random walkers. A possible choice for the corresponding transition probabilities is

$$P\left(\boldsymbol{\eta} \to \boldsymbol{\eta}^{\mathrm{O}}\right)(\boldsymbol{r}, k) = \frac{1}{Z}\delta\left(n(\boldsymbol{r}, k), n^{\mathrm{O}}(\boldsymbol{r}, k)\right)\,, \tag{1}$$

where $Z = \sum_{\boldsymbol{\eta}^{\mathrm{O}}(r,k)} \delta(n(\boldsymbol{r}, k), n^{\mathrm{O}}(\boldsymbol{r}, k))$ is a normalization factor. The Kronecker δ guarantees the mass conservation of this operator. For an intuitive understanding of the rule see Fig. 3.

The particular choice for the reorientation operator is one out of various possible ways to describe random motion by means of LGCA [4, 5]. Our choice greatly simplifies the subsequent analytical derivation of the equations describing the meso- and macroscopic evolution of the automaton.
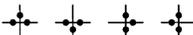
Fig. 3. Reorientation rule of random motion: The left column corresponds to the possible node densities $n(\boldsymbol{r}, \cdot)$, with node capacity $\tilde{b} = 4$. The central column provides all possible node configurations, while the right column indicates the respective transition probabilities (Eq. (1)).

2.2.3. Growth (R)

In our model, particles are allowed to proliferate if there is enough space. In particular, we assume a microscopic volume exclusion growth dynamics, where the maximum capacity is defined by the node capacity $\tilde{b}$. The effect of local volume exclusion on growth is also known as *carrying capacity-limited* or *contact-inhibited* growth.

Let us define the new occupation number after the application of the growth operator R:

$$\eta_i^R(\boldsymbol{r}, k) = \eta_i(\boldsymbol{r}, k) + R_i(\boldsymbol{r}, k). \tag{2}$$

The R_i models the birth of a new particle on a node $\boldsymbol{r}$ at time k. For the creation of a new particle on a node at least one free channel is required. This condition can be formulated in the following way:

$$R_i(\boldsymbol{r}, k) = \xi_i(\boldsymbol{r}, k)(1 - \eta_i(\boldsymbol{r}, k)), \tag{3}$$

where $\xi_i(\boldsymbol{r}, k)$'s are random Boolean variables, with $\sum_{i=1}^{\tilde{b}} \xi_i(\boldsymbol{r}, k) = 1$, and the corresponding probabilities are:

$$P(\xi_i(\boldsymbol{r}, k) = 1) = P\left(\{\eta_i^R(\boldsymbol{r}, k) = 1\} \wedge \{n(\boldsymbol{r}, k) > 0\}\right), \tag{4}$$

which is the probability that a newly created particle occupies a channel i and that there exists at least one particle on node $\boldsymbol{r}$. For analytical calculations, we assume the independency of these two events. Moreover, we define $r = P(\{\eta_i^R(\boldsymbol{r}, k) = 1\})$ as the probability of a new particle occupying the channel i. Together we have

$$P(\xi_i(\boldsymbol{r}, k) = 1) = P\left(\{\eta_i^R(\boldsymbol{r}, k) = 1\}\right) P(\{n(\boldsymbol{r}, k) > 0\}) = r\,\frac{n(\boldsymbol{r}, k)}{\tilde{b}}. \tag{5}$$

2.3. Microdynamical equations

The dynamics defined above are fully specified by the following microdynamical equations:

$$\eta_i(\boldsymbol{r} + m\boldsymbol{c}_i, k + \tau) \;=\; \sum_{j=1}^{\tilde{b}} \mu_j(\boldsymbol{r}, k)\eta_j^R(\boldsymbol{r}, k)\,, \qquad (6)$$

$$\eta_i^R(\boldsymbol{r}, k) \;=\; \eta_i(\boldsymbol{r}, k) + R_i(\boldsymbol{r}, k)\,.$$

The first equation (6) refers to the *redistribution* of particles on the velocity channels and the *propagation* to the neighboring nodes. The second equation coincides with (2). The $\mu_j(\boldsymbol{r}, k) \in \{0, 1\}$ are Boolean random variables which select only one of the $\tilde{b}$ terms of the r.h.s. of Eq. (6). Therefore, they should obey the relation $\sum_{j=1}^{\tilde{b}} \mu_j = 1$. In particular, for our specific choice (section 2.2.2) of the reorientation operator (O), the mean occupation ("current") of a channel j is: $\langle \mu_j \rangle = 1/\tilde{b}$, $j = 1, \dots, \tilde{b}$.

Finally, we define some useful notations which are employed in the rest of the text: $f_i(\boldsymbol{r}, k) = \langle \eta_i(\boldsymbol{r}, k) \rangle$ as the *single particle distribution* or mean occupation number of a channel at a node $\boldsymbol{r}$ and time t, and the *mean node density* as $\rho(\boldsymbol{r}, k) = \langle n(\boldsymbol{r}, k) \rangle = \sum_{i=1}^{\tilde{b}} f_i(\boldsymbol{r}, k)$. In the following, we introduce the mean-field approximation of our growth LGCA.

3. Mean-field analysis

This section introduces the mean-field (MF) analysis of the above defined growth LGCA. The main idea of the mean-field approximation is to replace the description of many-particle interactions by a single particle description based on an average or effective interaction. Thereby, any multi-particle problem can be replaced by an effective problem, that can be stated in the form of a macroscopic description such as an ordinary differential equation (ODE) or a PDE.

We introduce the derivation of the mean-field approximation under the assumption of a well-stirred case (for which the diffusion coefficient diverges) and a spatially distributed case, *i.e.* a finite diffusion strength $(< \infty)$ is assumed.

3.1. Well-stirred system

Here, we derive a mean-field approximation of our LGCA under the assumption of a well-stirred system [11]. In automaton terms, within one time step $(k, k+\tau)$ the transport operator (6), which randomly reshuffles the particles on the velocity channels and propagates them to the neighboring

nodes, is repeatedly applied until the system is homogenized and relaxes to a single binomial distribution over the lattice, *i.e.* $(P \circ O)^{l_D}$, where $l_D \to \infty$ [19]. Phenomenologically, a well-stirred system corresponds to a divergent diffusion coefficient, *i.e.* $D \to \infty$. That means that the characteristic time of growth is much slower than the characteristic time of particle motion (diffusion time). Neglecting all spatial correlations, we define:

$$P_{\text{binom}}(n(\boldsymbol{r}), \rho) = \frac{\tilde{b}!}{(\tilde{b} - n(\boldsymbol{r}))! n(\boldsymbol{r})!} \left(\frac{\rho}{\tilde{b}}\right)^{n(\boldsymbol{r})} \left(1 - \frac{\rho}{\tilde{b}}\right)^{\tilde{b} - n(\boldsymbol{r})}, \quad \forall \boldsymbol{r} \in \mathcal{L}, \quad (7)$$

where ρ is the average node density of the lattice, *i.e.* $\rho = \sum_{\boldsymbol{r} \in \mathcal{L}} n(\boldsymbol{r})/|\mathcal{L}|$. We drop the temporal and the spatial argument since the well-stirred system assumes a spatially homogeneous node density distribution for each time interval $(k, k + \tau)$. The joint probability of the set of node configurations $\{\boldsymbol{\eta}(\boldsymbol{r})\}_{\boldsymbol{r} \in \mathcal{N}}$, where $\mathcal{N} = \{\boldsymbol{r} \in \mathcal{L} | n(\boldsymbol{r}) \neq 0\} \subseteq \mathcal{L}$ is the set of occupied nodes of the lattice $\mathcal{L}$, is:

$$P(\{\boldsymbol{\eta}(\boldsymbol{r})\}_{\boldsymbol{r} \in \mathcal{N}}) = \prod_{\boldsymbol{r} \in \mathcal{N}} P_{\text{binom}}(n(\boldsymbol{r}), \rho). \quad (8)$$

By the application of the reaction step, the node density may change $n(\boldsymbol{r}) \to n(\boldsymbol{r}) + 1$ with the transition probability $p^+(n(\boldsymbol{r}))$. Let α_+ denote the set of nodes that gain a particle, where this event is realized by the probability:

$$P(\alpha_+) = \sum_{\{\boldsymbol{\eta}(\boldsymbol{r})\}} P(\alpha_+ | \{\boldsymbol{\eta}(\boldsymbol{r})\}) P(\{\boldsymbol{\eta}(\boldsymbol{r})\}). \quad (9)$$

Here, $P(\alpha_+ | \{\boldsymbol{\eta}(\boldsymbol{r})\})$ is the conditional probability for the transition $n(\boldsymbol{r}) \to n(\boldsymbol{r}) + 1$ from a given configuration $\{\boldsymbol{\eta}(\boldsymbol{r})\}_{\boldsymbol{r} \in \mathcal{N}}$. Therefore,

$$P(\alpha_+ | \{\boldsymbol{\eta}(\boldsymbol{r})\}) = \prod_{\boldsymbol{r} \in \alpha_+} p^+(n(\boldsymbol{r})) \prod_{\boldsymbol{r} \in (\mathcal{N} - \alpha_+)} \left(1 - p^+(n(\boldsymbol{r}))\right). \quad (10)$$

Summing over all possible configurations $\{\boldsymbol{\eta}(\boldsymbol{r})\}_{\boldsymbol{r} \in \mathcal{N}}$ in (9), we obtain the following binomial distribution:

$$P(\alpha_+) = \frac{|\mathcal{N}|!}{|\alpha_+|!(|\mathcal{N}| - |\alpha_+|)!} (P^+)^{|\alpha_+|} \left(1 - P^+\right)^{|\mathcal{N}| - |\alpha_+|}, \quad (11)$$

where the prefactor takes into account all the possible choices of assigning the α_+ transitions $n \to n+1$ to possible positions on the lattice and the $|\cdot|$ denotes the cardinality of a set. The probabilities $P^+ = \sum_n p^+(n) P_{\text{binom}}(n, \rho)$ are the averages of the transition probabilities $p^+(n)$ over the binomial distribution on the lattice $\mathcal{L}$.

Therefore, the expected value of the net change in the node density during one time step becomes:

$$\langle \Delta \rho \rangle_{\mathrm{MF}} = \rho(k+\tau) - \rho(k) = \frac{1}{|\mathcal{N}|} \sum_{|\alpha_+| \le |\mathcal{N}|} \alpha_+ P(\alpha_+) = P^+ = F(\rho), \quad (12)$$

where $F(\rho)$ is the mean-field growth law for a single node. Following the definition of the automaton's reaction rule (3), the mean-field growth term is:

$$F(\rho) = r\rho \left(1 - \frac{\rho}{\tilde{b}} \right) . \quad (13)$$

The transition of a microscopical process to a macroscopic description requires a *temporal scaling* relation between the macroscopic and microscopic variables. We assume a small parameter $\epsilon \ll 1$ that scales the time variable t:

$$t = \epsilon k . \quad (14)$$

Using the Taylor expansion $\rho(k+\tau) = \rho(k) + \epsilon\tau\partial_t\rho(t)|_{t=k}$ and rewriting equation (12) in continuous variables:

$$\partial_t \rho = \frac{r}{\epsilon\tau} \rho \left(1 - \frac{\rho}{\tilde{b}} \right) , \quad (15)$$

which is the *logistic growth* equation [15]. Note that $0 < \epsilon\tau \ll 1$. This means that the ratio $r/\epsilon\tau < \infty$ should be finite. Thus, the growth rate should be scaled as $r \propto \epsilon\tau \ll 1$, which means that equation (15) is valid for small growth rates. Therefore, we have shown that our growth process under the mean-field and the well-stirred system assumptions behaves macroscopically as the logistic equation (15).

3.2. Spatially distributed system

Now, we demonstrate how to derive a spatio-temporal mean-field approximation of our growth automaton for a spatially distributed system. In this case, we consider the space in our mean-field analysis which allows for an average description of the single node behavior. From this average node description, we can extrapolate the macroscopic behavior of the system. To do that we employ an appropriate spatio-temporal scaling method.

The average change of the occupation number of channel i, where $i = 1, \dots, \tilde{b}$, is:

$$f_i(\boldsymbol{r} + m\boldsymbol{c}_i, k+\tau) - f_i(\boldsymbol{r}, k) = \langle \eta_i(\boldsymbol{r} + m\boldsymbol{c}_i, k+\tau) - \eta_i(\boldsymbol{r}, k) \rangle_{\mathrm{MF}} . \quad (16)$$

Using the mean-field approximation, where all spatial correlations are neglected, and combining equations (2), (6) and (16), we obtain:

$$f_i(\mathbf{r}+m\mathbf{c}_i, k+\tau) - f_i(\mathbf{r}, k) = \sum_{j=1}^{\tilde{b}} \Omega_{ij} f_j(\mathbf{r}, k) + \sum_{j=1}^{\tilde{b}} (\delta_{ij}+\Omega_{ij})\bar{R}_i(\mathbf{r}, k)\,, \quad (17)$$

where the matrix $\Omega_{ij} = 1/\tilde{b} - \delta_{ij}$ is the transition matrix of the underlying shuffling process. Moreover, we assume that the mean-field growth term is independent of the particle direction, i.e. $\bar{R}_i = F(\rho)/\tilde{b}$, where $F(\rho)$ is the mean-field growth term for a single node. The mean-field growth term is:

$$\bar{R}_i(\boldsymbol{r}, k) = r f_i(\boldsymbol{r}, k)(1 - f_i(\boldsymbol{r}, k))\,. \quad (18)$$

In order to derive the macroscopic dynamics, we use the Chapman–Enskog methodology, described in [4]. In the following, we apply the parabolic (or diffusive) spatio-temporal scaling

$$\boldsymbol{x} = \epsilon\boldsymbol{r} \quad \text{and} \quad t = \epsilon^2 k\,, \quad (19)$$

where $(\boldsymbol{x}, t)$ are the continuous variables as $\epsilon \to 0$. The parabolic scaling provides the long-term macroscopic dynamics of a diffusion-based process. The small parameter ϵ is defined as the ratio of the microscopic mean free path, i.e. the microscopic jump m of a particle within a microscopic time step τ, and the macroscopic length scale, i.e. the length of the domain L:

$$\epsilon = \frac{m}{L} \ll 1\,. \quad (20)$$

Now, we suppose an asymptotic solution of the single particle distribution f_i in terms of the parameter ϵ:

$$f_i = f_i^{(0)} + \epsilon f_i^{(1)} + \epsilon^2 f_i^{(2)} + \mathcal{O}(\epsilon^3)\,. \quad (21)$$

An important aspect is the scaling of the growth term. We assume that particle proliferation occurs at a much slower time scale than particle motion. Thus the growth process can be considered as a perturbation of the particle transport. That means that the main process is particle diffusion (as it is also shown below) and the growth rate should be scaled according to the macroscopic time scaling, i.e.:

$$\bar{R}_i \to \epsilon^2 \tilde{R}_i\,. \quad (22)$$

The above relation implies that the macroscopic growth rate scales $\tilde{r}_m = \epsilon^2 r$, where the microscopic rate is $r \propto \mathcal{O}(1)$. Therefore, our approach is valid only for very low growth rates.

Moreover, the Chapman–Enskog procedure allows us to derive an asymptotic solution for $f_i(\boldsymbol{r}, k)$ (see Appendix), *i.e.*

$$f_i(\boldsymbol{r}, k) = \frac{\rho(\boldsymbol{r}, k)}{\tilde{b}} - \epsilon \frac{m}{\tilde{b}} (\boldsymbol{c}_i \cdot \nabla) \rho(\boldsymbol{r}, k) + \epsilon^2 \frac{m^2}{2\tilde{b}^2} \left[\tilde{b} (\boldsymbol{c}_i \cdot \nabla)^2 - 2\nabla^2 \right] \rho(\boldsymbol{r}, k) \,. \tag{23}$$

Intuitively, we understand the above equation as a perturbation of the homogeneous equilibrium solution $\rho(\boldsymbol{r}, k)/\tilde{b}$ scaled by the parameter ϵ.

Collecting the equal $\mathcal{O}(\epsilon^2)$ terms, we can formally derive a spatio-temporal mean-field macroscopic approximation (see Appendix):

$$\partial_t \rho = \frac{m^2}{\tilde{b}\tau} \nabla^2 \rho + \frac{1}{\tau} F(\rho) \,, \tag{24}$$

where $F(\rho)$ is the macroscopic growth law, *i.e.*

$$F(\rho) = \tilde{r}_m \rho \left(1 - \frac{\rho}{\tilde{b}} \right) \,. \tag{25}$$

By non-dimensionalizing the above equation, we can readily obtain the widely used *Fisher–Kolmogorov (FK)* equation [13].

4. Mean-field approximations and macroscopic behavior

In the previous section, we presented two types of mean-field approximations of LGCA. The question is which approach is more appropriate to describe the automaton's macroscopic behavior. In this section, we provide a comparison of the two mean-field approaches and try to identify their limitations. In particular, we use the well-stirred and the spatially distributed mean-field approximations to gain insight into: *(i)* the spatio-temporal pattern formation of the LGCA and *(ii)* the behavior of important macroscopic observables, such as *total number of particles* ($\bar{\rho}(t)$) and the *per capita growth rate* (γ).

Based on the mean-field approximation of the well-stirred system, we have derived an ODE (15) that allows us to calculate the net change in the node density for any given time. The total number of particles in the system is

$$\bar{\rho}(t) = \sum_{\boldsymbol{r} \in \mathcal{L}} \rho(t) = |\mathcal{L}| \rho(t) \,.$$

Thus, using equation (15), the time evolution of the total number of particles in the system is given by the equation

$$\bar{\rho}(t) = \frac{C}{1 + \left(\frac{C}{\bar{\rho}_0} - 1 \right) e^{-\frac{r}{\epsilon\tau} t}} \,, \tag{26}$$

where $\bar{\rho}_0$ is the initial total number of particles in the system and $C = \tilde{b}|\mathcal{L}|$ is the total capacity of the lattice $\mathcal{L}$. The *per capita* growth rate is defined as the average number of offsprings per individual for a given time, *i.e.*

$$\gamma = \frac{\Delta \bar{\rho}(t)}{\bar{\rho}(t)} \,. \tag{27}$$

The total number of produced particles is

$$\Delta \bar{\rho}(t) = \frac{d\bar{\rho}(t)}{dt} = r\bar{\rho} \left(1 - \frac{\bar{\rho}}{\tilde{b}} \right) \,.$$

Therefore, the *per capita* growth rate for the well-stirred system is:

$$\gamma_{t\mathrm{MF}} = r \left(1 - \frac{\bar{\rho}}{\tilde{b}} \right) \,. \tag{28}$$

The well-stirred MF approximation is inappropriate for the analysis of the spatio-temporal pattern formation, since space is not considered in equation (26).

Now we demonstrate how the macroscopic description under the assumption of finite diffusion strength (25) allows for an analysis of the spatio-temporal pattern formation in the growth LGCA. The pattern evolving in simulations from a localized initial occupation is an isotropically growing disc (Fig. 4). The isotropy of the system becomes apparent in the Chapman–Enskog expansion, in particular by comparing the mean fluxes of particles along x–y directions and calculating the total mean flux [10], *i.e.*:

$$|\langle \boldsymbol{J}_{x+} \rangle - \langle \boldsymbol{J}_{y+} \rangle| = |\boldsymbol{c}_1 f_1 - \boldsymbol{c}_2 f_2| = 0 \wedge \langle \boldsymbol{J} \rangle = \sum_{i=1}^{\tilde{b}} \boldsymbol{c}_i f_i = 0 \,. \tag{29}$$
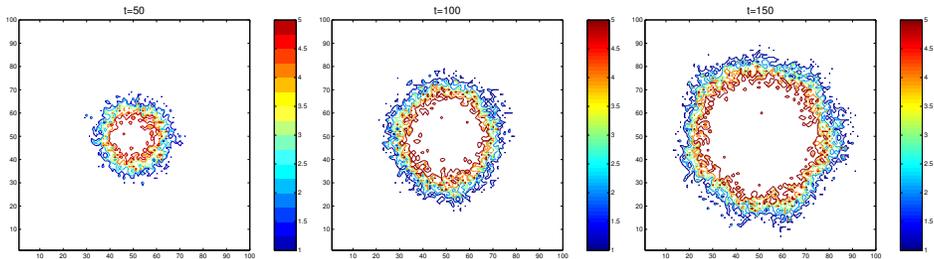

Fig. 4. Typical simulations of the spatio-temporal evolution of the LGCA growth process starting from a localized initial occupation. The three pictures show simulation snapshots for subsequent time steps. The colors indicate the node density.

Furthermore, simulations indicate a moving front along which the occupancy of the initially empty nodes is increasing from zero particles to the maximum capacity $\tilde{b}$. This behavior is predicted by the FK equation (24), which is known to produce a front where the stable phase ($\rho(x,t) = \tilde{b}$) propagates towards the unstable one ($\rho(x,t) = 0$).

In order to calculate the total number of particles and the per capita growth rate, we assume that the system evolves for asymptotically long times and the initial front is sufficiently steep. In this case the speed of the front relaxes to its asymptotic value $c^* = c_{\min} = 2\sqrt{m^2/\tilde{b}r}$ [13]. Additionally, the above assumptions allow us to consider that the resulting front is extremely steep (sharp interface between the stable and the unstable phase).

Now, we can calculate the total number of particles. Using the relation, $\bar{\rho}(t) = \tilde{b}\pi R(t)^2$, where the radius grows as $R(t) = c^*t$, the total number of particles is:

$$\bar{\rho}(t) = 4\pi m^2 r t^2 \,. \tag{30}$$

The *per capita* growth rate is given by the relation $\gamma = \Delta\bar{\rho}(t)/\bar{\rho}(t)$, where $\Delta\bar{\rho}(t) = d\bar{\rho}(t)/dt = 8\pi m^2 r t$ is the change of $\bar{\rho}(t)$. Then, it follows that

$$\gamma_{\mathrm{spMF}} \sim \frac{1}{\sqrt{\bar{\rho}(t)}} \,. \tag{31}$$
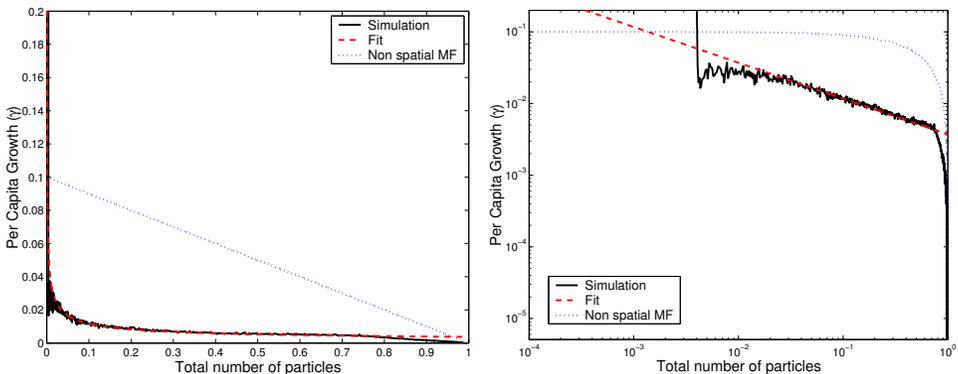

Fig. 5. Evolution of the *per capita* growth γ as a function of the total population density $\bar{\rho}$. The individual growth rate γ derived from the LGCA simulations decreases rapidly for increasing population densities. The behavior of γ can be fitted by a curve $\bar{\rho}^{-1/2}$, as it is calculated in our spatio-temporal MF analysis (31). The temporal MF (28) completely fails to follow the actual LGCA dynamics. The log–log plot (right figure) allows to better distinguish the better the fit and the simulation curves, especially for low $\bar{\rho}$.

In Fig. 5, we show the behavior of the *per capita* growth rate of both mean-field approximations in comparison with actual LGCA simulation results. We observe that $\gamma_{t\text{MF}}$ fails to match exactly the *per capita* growth of the simulations. The per capita growth γ_{spMF}, derived from the spatio-temporal MF, offers a better insight into the actual growth dynamics, since it recovers qualitatively the scaling (31) of the *per capita* growth rate derived from simulations. However, the γ_{spMF} does not agree quantitatively with the actual *per capita* growth. In the next section, we discuss this disagreement.

5. Discussion

A recent review [2] of a book on cellular automaton models of biological pattern formation [5] has questioned the potential of a mean-field analysis of CA in gaining insight into the automaton's spatio-temporal behavior. This objection motivated us to present the applications of the mean-field analysis to a stochastic growth process, formulated in terms of a LGCA model. In particular, we have analyzed the stochastic LGCA model under the mean-field assumption in the cases of a well-stirred and a spatially distributed system, respectively. Then we have derived the corresponding macroscopic deterministic differential equations and we used them to gain insight into the spatio-temporal behavior of the underlying growth process. In contrast to the well-stirred assumption, the spatially distributed assumption leads to a satisfactory description of the system's spatial pattern formation and recovers the scaling laws of important macroscopic measures, such as particle number and *per capita* growth rate.

Altogether, the derived spatio-temporal mean-field description characterizes the stochastic growth process. However, the approximation fails to provide exact quantitative predictions of those properties which rely on higher order spatial correlations. This is due to the nature of the mean-field approximation which neglects spatial correlations, together with the sharp interface assumption. The quantitative predictions of the analytical theory could be improved by the exact calculation of the invasive front or the extension of the mean-field approximation [9]. Both topics are challenging research fields but their discussion is beyond the scope of this paper.

Appendix

The Chapman–Enskog method for LGCA is described in detail in [4]. Introducing the spatio-temporal scaling relation Eq. (19) and replacing the first part of equation (17) by its Taylor expansion, we obtain:

$$f_i(\boldsymbol{r}+m\boldsymbol{c}_i\,,k+\tau)-f_i(\boldsymbol{r},k)=$$

$$\left(\epsilon^2\tau\partial_t+\epsilon^4\frac{\tau^2}{2}\partial_{tt}+\epsilon m(\boldsymbol{c}_i\cdot\nabla)+\epsilon^2\frac{m^2}{2}(\boldsymbol{c}_i\cdot\nabla)^2+\ \epsilon^3\tau m\partial_t(\boldsymbol{c}_i\cdot\nabla)\right)f_i(\boldsymbol{r},k)\,. \tag{32}$$

Furthermore, we assume an asymptotic solution of the single particle distribution in the form of (23), *i.e.*

$$f_i(\boldsymbol{r},k) = \sum_{l=0}^{n} \epsilon^l f_i^{(l)}(\boldsymbol{r},k) + \mathcal{O}(n+1)\,. \tag{33}$$

Moreover, we consider that the particle growth is scaled as:

$$\bar{R}_i \to \epsilon^2 \tilde{R}_i\,. \tag{34}$$

The macroscopic quantities of interest are the particle densities $\rho = \sum_i f_i^{(0)}$, with the assumption $\sum_i f_i^{(l)} = 0$, if $l \geq 1$.

The next step is to insert Eqs. (22) and (32) into (17) and to collect the terms of equal ϵ order:

$$\mathcal{O}(\epsilon^0): \ \sum_j \Omega_{ij} f_j^{(0)} = 0\,, \tag{35}$$

$$\mathcal{O}(\epsilon^1): \ m(\boldsymbol{c}_i \cdot \nabla) f_j^{(0)} = \sum_j \Omega_{ij} f_j^{(1)}\,, \tag{36}$$

$$\mathcal{O}(\epsilon^2): \tau\partial_t f_i^{(0)}+m(\boldsymbol{c}_i\cdot\nabla) f_i^{(1)}+\frac{m^2}{2}(\boldsymbol{c}_i\cdot\nabla)^2 f_i^{(0)}=\sum_j \Omega_{ij} f_j^{(2)}+\tilde{R}_i\,. \tag{37}$$

The solutions of the above equations (35), (36), (37) are based on the properties of the transition matrix Ω [4] and the results are:

$$f_j^{(0)} = \frac{\rho}{\tilde{b}},\tag{38}$$

$$f_j^{(1)} = -\frac{m}{\tilde{b}}(\boldsymbol{c}_i \cdot \nabla)\rho.\tag{39}$$

To obtain a macroscopic equation, we sum equation (37) over i; it follows:

$$\tau\partial_t \sum_i f_i^{(0)} + m\sum_i (\boldsymbol{c}_i \cdot \nabla) f_i^{(1)} + \frac{m^2}{2}\sum_i (\boldsymbol{c}_i \cdot \nabla)^2 f_i^{(0)} = \sum_{ij}\Omega_{ij} f_j^{(2)} + \sum_i \tilde{R}_i.\tag{40}$$

Performing the above summation (using the property of the transition matrix $\sum_{ij}\Omega_{ij} = 0$ and the property of the lattice tensor[2] $\sum_i c_{i\alpha}c_{i\beta} = d\delta_{\alpha\beta}$, where d is the dimension of the system), yields the following reaction-diffusion equation (24):

$$\partial_t\rho = \frac{m^2}{\tau\tilde{b}}\nabla^2\rho + \frac{1}{\tau}F(\rho),\tag{41}$$

where $F(\rho)$ is the macroscopic growth law.

From Eqs. (24) and (37), we can obtain an expression for $f_i^{(2)}$:

$$f_i^{(2)}(\boldsymbol{r}, k) = \frac{m^2}{2\tilde{b}^2}\left[\tilde{b}(\boldsymbol{c}_i \cdot \nabla)^2 - 2\nabla^2\right]\rho(\boldsymbol{r}, k).\tag{42}$$

Thus the asymptotic solution of the single particle distribution is:

$$\begin{aligned}f_i(\boldsymbol{r}, k) &= \frac{\rho(\boldsymbol{r}, k)}{\tilde{b}} - \epsilon\frac{m}{\tilde{b}}(\boldsymbol{c}_i \cdot \nabla)\rho(\boldsymbol{r}, k)\\ &\quad + \epsilon^2\frac{m^2}{2\tilde{b}^2}\left[\tilde{b}(\boldsymbol{c}_i \cdot \nabla)^2 - 2\nabla^2\right]\rho(\boldsymbol{r}, k).\end{aligned}\tag{43}$$

---

[2] The automaton's spatial and velocity discretizations are related to the definition of the lattice tensor. The velocity vectors $\boldsymbol{c}_i$ yield an orthogonal basis for the construction of the lattice tensors. The lattice tensors contain all the isotropy and symmetry properties of the automaton's space $\mathcal{L}$ [14].

List of symbols

Symbol	Explanation
$\mathcal{L} \subset \mathbb{Z}^d$	d-dimensional regular lattice
$\lvert \cdot \rvert$	cardinality of a set
$L_i, \ i = 1, \dots, d$	length of the lattice along i^{th} dimension
$(\boldsymbol{r}, k) \in \mathbb{N}^2$	discrete spatio-temporal variables
$\boldsymbol{c}_i \in \mathbb{Z}^d, \ i = 1, \dots, b$	velocity channel vector
$\beta \in \mathbb{N}_0 = \mathbb{N} \cup \{0\}$	number of rest channels
b	coordination number
$\tilde{b} = b + \beta$	total number of channels
$\boldsymbol{\eta}(\boldsymbol{r}) \in \{0,1\}^{\tilde{b}}$	node configuration
$\eta_i(\boldsymbol{r}) \in \{0,1\}, i = 1, \dots, \tilde{b}$	occupation number
$n(\boldsymbol{r}, k) \in \{0, \dots, \tilde{b}\}$	node density
$P(\cdot)$	probability measure
$m \in \mathbb{N}$	single particle speed
$\tau \in \mathbb{N}$	automaton's time step
P	propagation operator
O	reorientation operator
Ω	transition matrix of LBE
$\rho(\boldsymbol{r}, k) \in [0, \tilde{b}]$	mean node density
$(\boldsymbol{x}, t) \in \mathbb{R}^2 \times \mathbb{R}_+$	continuous spatio-temporal variables
$\epsilon \ll 1$	scaling parameter
R	growth operator
$\boldsymbol{J}(\boldsymbol{\eta}(\boldsymbol{r}, k))$	node flux

REFERENCES

[1] N. Boccara, *Modeling Complex Systems*, Springer, 2004.

[2] M. Boerlijst, *Math. Biosc.* **200**, 118 (2006).

[3] J.P. Boon, D. Dab, R. Kapral, A. Lawniczak, *Phys. Rep.* **273**, 55 (1996).

[4] B. Chopard, M. Droz, *Cellular Automata Modeling of Physical Systems*, Cambridge University Press, Cambridge 1998.

[5] A. Deutsch, S. Dormann, *Cellular Automaton Modeling of Biological Pattern Formation*, Birkhauser, 2005.

[6] G.D. Doolen, *Lattice Gas Methods for Partial Differential Equations*, Addison-Wesley, New York 1990.

[7] R.A. Fisher, *The Genetical Theory of Natural Selection*, Oxford University Press, 1930.

[8] U. Frisch, D. d'Humieres, B. Hasslacher, P. Lallemand, Y. Pomeau, J.P. Rivet, *Compl. Syst.* **1**, 649 (1987).

[9] H. Hatzikirou, L. Brusch, C. Schaller, M. Simon, A. Deutsch, *Comput. Math. Appl.* in print.

[10] H. Hatzikirou, A. Deutsch, *Curr. Top. Dev. Biol.* **81**, 401 (2008).

[11] R. Kapral, X. Wu, *Physica D* **103**, 314 (1997).

[12] A.T. Lawniczak, *Transp. Theor. Stat. Phys.* **29**, 261 (2000).

[13] J. Murray, *Mathematical Biology I: An Introduction*, Springer, 2001.

[14] D.H. Rothman, S. Zaleski, *Rev. Mod. Phys.* **66(4)**, 1417 (1994).

[15] R.F. Verhulst, *Nouv. mm. de l'Academie Royale des Sci. et Belles-Lettres de Bruxelles*, **18**, 1 (1845).

[16] J. von Neumann, *Theory of Self-Reproducing Automata*, Urbana, University of Illinois Press, 1966.

[17] D.A. Wolf-Gladrow, *Lattice-Gas Cellular Automata and Lattice Boltzmann Models — An Introduction*, Springer, 2005.

[18] S. Wolfram, *A New Kind of Science*, Wolfram Media, Inc., 2002.

[19] X. Wu, R. Kapral, *J. Chem. Phys.* **100**, 5936 (1994).